International Journal of Mass Spectrometry 283 (2009) 35–47

Contents lists available at ScienceDirect

International Journal of Mass Spectrometry

journal homepage: www.elsevier.com/locate/ijms

Inductive effects on cation–π interactions: Structures and bond dissociation energies of alkali metal cation–halobenzene complexes

Nuwan Hallowita, Estima Udonkang, Chunhai Ruan, C.E. Frieler, M.T. Rodgers*

Department of Chemistry, Wayne State University, 5101 Cass Avenue, 33 Chemistry, Detroit, MI 48202, United States

ARTICLE INFO

Article history:
Received 25 November 2008
Received in revised form 13 January 2009
Accepted 13 January 2009
Available online 22 January 2009

In honor of M.T. Bowers on the occasion of his 70th birthday, in thanks for his numerous contributions to gas-phase ion chemistry, ion mobility and mass spectrometry, and in appreciation for his scientific mentoring and friendship.

Keywords:
Alkali metal cations
Cation–π interactions
Collision-induced dissociation
Guided ion beam tandem mass spectrometry
Halobenzenes

ABSTRACT

The influence of halogenation on cation–π interactions is investigated both experimentally and theoretically. Bond dissociation energies (BDEs) of alkali metal cation–halobenzene complexes, $M^+(C_6H_5X)$, are determined using threshold collision-induced dissociation techniques in a guided ion beam tandem mass spectrometer, where $M^+ = Na^+$ and K^+, and X = Cl, Br, and I. The primary dissociation pathway for all systems is endothermic loss of the neutral halobenzene from the cation–π complex. In addition, minor production of the ligand exchange product, M^+Xe, is also observed. At elevated energies elimination of NaX is also observed for the $Na^+(C_6H_5Br)$ and $Na^+(C_6H_5I)$ systems. Ab initio calculations at the B3LYP/6-31+G* level of theory are used to determine the structures of the neutral π-ligands and cation–π complexes. Theoretical BDEs are determined from single point calculations at the MP2(full)/6-311+G(2d,2p) level using the B3LYP/6-31+G* optimized geometries. Good agreement between the theoretical and experimental BDEs is found in all cases. The trends in the BDEs of the $M^+(C_6H_5X)$ complexes are explained in terms of the varying magnitude of the electrostatic interactions in these complexes elucidated from a binding parameter model. Comparisons are also made to BDEs previously determined for the analogous $M^+(C_6H_6)$ and $M^+(C_6H_5F)$ complexes to examine the inductive effects of the halogen substituent on the strength of the cation–π interaction.

1. Introduction

As with hydrophobic interactions, van der Waals forces, and hydrogen bonds, cation–π interactions represent another type of noncovalent interaction that plays important roles in protein structure determination [1–4] and molecular recognition processes associated with the functions of ion channels and enzymes [5–11]. Cation–π interactions may occur between a cation and a neutral or anionic π-electron system; however cation–π interactions involving neutral π-electron systems are of greater relevance to biological processes [12]. To date numerous experimental studies have investigated cation–π interactions, and in particular have been devoted to the characterization of the strength of these interactions [13–31]. In addition, calculations of the structures and the bond dissociation energies (BDEs) of cation–π complexes [9,13–39] and electrostatic potential maps [29,31] have often been performed to complement the experimental work.

Most studies of cation–π interactions have been carried out in the gas phase or in a pseudo aqueous environment simulated by partial hydration of the cation. In these studies, it has been found that the more hydrated the metal cation, the less susceptible it is to a cation–π interaction [40]. Cabarcos et al. used such partial hydration studies to demonstrate ion selectivity in ion channels [41]. They attributed the selectivity for K^+ over Na^+ in potassium ion channels to differences in the energetics of solvation of these metal cations. Their studies showed that K^+ exhibits a greater binding affinity for benzene than water molecules in the first solvation shell. However, the sodium cation does not display such behavior, as the water molecules are not as readily displaced by benzene. This difference in their interactions confers selectivity for potassium cations over sodium cations [3]. Gas-phase studies also provide insight into the intrinsic contributions to the binding in cation–π interactions, which are dependent on both the specific metal cation and π-electron system. Studies in the gas phase provide a measure of the cation–π interaction in low polarity environments, which make up the bulk of cation–π interactions operative in biological systems.

The strength and specificity of cation–π interactions are determined by the electrostatic forces between the cation and π system involved, i.e., ion-dipole, ion-quadrupole, and ion-induced dipole interactions. Of these three, the ion-quadrupole interaction has been shown to dominate cation–π interactions in benzene systems [10,18–31,42]. However the relative contributions to the binding

* Corresponding author. Tel.: +1 3135772431; fax: +1 3135778822.
E-mail address: mrodgers@chem.wayne.edu (M.T. Rodgers).

1387-3806/$ – see front matter © 2009 Elsevier B.V. All rights reserved.
doi:10.1016/j.ijms.2009.01.006

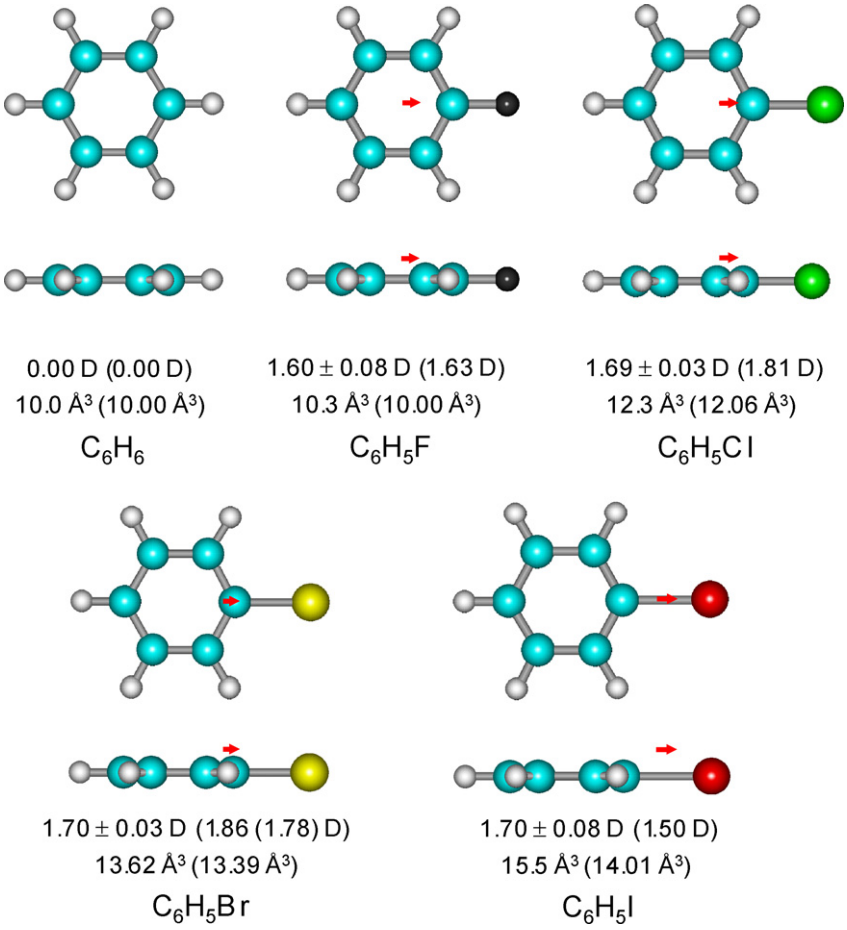

Fig. 1. Geometry-optimized structures of C_6H_6, C_6H_5F, C_6H_5Cl, C_6H_5Br, and C_6H_5I. Measured [45] (and calculated) dipole moments in Debye are shown. Properly scaled and oriented dipole moment vectors are shown as arrows as determined from the theoretical calculations. Measured [45] (and calculated) isotropic molecular polarizabilities in Å^3 are also shown.

are likely to be strongly influenced by substituents. Electropositive substituents enhance the cation–π interaction, while electronegative substituents tend to destabilize it [43]. Therefore, fundamental characterization of the factors that influence the strength and specificity of cation–π interactions is necessary and will prove useful in understanding the detailed roles these interactions play in biological systems and for optimization of technological applications that make use of cation–π interactions. The halobenzenes provide a simple deviation from the idealized symmetric structures of cation–π interactions between benzene and metal cations. In addition, halogen bonds occur naturally where they function as stabilizing intermolecular interactions in a C–X···O–Y bond fashion, where X is a halogen substituent, and O–Y a carbonyl, hydroxyl, charged carboxylate or phosphate group [44]. The electrostatic potential energy maps for the halobenzenes reveal that the strength of the X···O interaction should increase as the size of the halogen increases due to an increase in the polarizability [44], and to a lesser extent the dipole moment of the π system.

In this study, we explore the influence of inductive effects on cation–π interactions by examining cation–π complexes to several aromatic ligands containing electron-withdrawing substituents, the halobenzenes, C_6H_5X, where X = Cl, Br, and I. The alkali metal cations examined in the present study include Na^+ and K^+, which were selected due to their abundance and significance in biological systems. The present results are compared to the analogous benzene [16] and fluorobenzene [21] systems previously examined. In addition, a binding parameter analysis designed to elucidate the absolute and relative contributions that ion-dipole, ion-quadrupole, and ion-induced dipole interactions contribute to the binding is performed. In particular, the inductive effects of halogen substituents on the cation–π interaction are examined. The structures of benzene (C_6H_6), fluorobenzene (C_6H_5F), chlorobenzene (C_6H_5Cl), bromobenzene (C_6H_5Br), and iodobenzene (C_6H_5I) along with their measured [45] and calculated dipole moments and isotropic molecular polarizabilities are shown in Fig. 1.

2. Experimental and theoretical

2.1. Experimental protocols

Cross sections for collision-induced dissociation (CID) of six $M^+(C_6H_5X)$ complexes, where $M^+ = Na^+$ and K^+, and X = Cl, Br, and I are measured using a guided ion beam tandem mass spectrometer that has been described in detail previously [46]. The complexes are formed by condensation of the alkali metal cation and neutral halobenzene ligand in a flow tube ion source operating at pressures in the range of 0.5–0.8 Torr. These complexes are collisionally stabilized and thermalized by in excess of 10^5 collisions with the He and Ar bath gases such that the internal energies of the ions emanating from the source region are expected to be well described by a Maxwell–Boltzmann distribution at room temperature. The ions are effusively sampled, focused, accelerated, and focused into a magnetic sector momentum analyzer for mass analysis. Mass-selected ions are decelerated to a desired kinetic energy and focused into an octopole ion guide. The octopole passes through a static gas cell containing Xe [47–49] at sufficiently low pressure

(0.05–0.20 mTorr) to ensure that multiple ion-neutral collisions are improbable. The octopole ion guide acts as an efficient trap for ions in the radial direction [50–52]. Therefore, loss of scattered reactant and product ions in the octopole region is almost entirely eliminated. Products and unreacted beam ions drift to the end of the octopole, where they are focused into a quadrupole mass filter for mass analysis, and subsequently detected with a secondary electron scintillation detector and standard pulse counting techniques.

2.1.1. Data handling

Measured ion intensities are converted to absolute cross sections using a Beer's law analysis as described previously [53]. Uncertainties in the absolute cross-section magnitudes are estimated to be ±20%, while the relative uncertainties are approximately ±5%, and result from errors in the pressure measurement and the length of the interaction region.

Ion kinetic energies in the laboratory frame, E_{lab}, are converted to energies in the center-of-mass frame, E_{CM}, using the formula $E_{CM} = E_{lab}m/(m+M)$, where M and m are the masses of the ionic and neutral reactants, respectively. All energies reported below are in the center-of-mass frame unless otherwise noted. The absolute zero and distribution of the ion kinetic energies are determined using the octopole ion guide as a retarding potential analyzer as previously described [53]. The distribution of ion kinetic energies is nearly Gaussian with a fwhm between 0.3 and 0.5 eV (lab) for these experiments. The uncertainly in the absolute energy scale is ±0.05 eV (lab).

Because multiple ion-neutral collisions can alter the shape of the CID cross sections, particularly in the threshold regions, the CID cross section for each complex was measured twice at three nominal pressures (0.05, 0.10, and 0.20 mTorr). Data free from pressure effects are obtained by extrapolating to zero pressure of the neutral reactant, Xe, as described previously [47]. The zero-pressure-extrapolated cross sections subjected to thermochemical analysis are therefore the result of single bimolecular encounters.

2.2. Theoretical calculations

To obtain model structures, vibrational frequencies, and energetics for neutral benzene and the halobenzenes and the complexes of benzene and the halobenzenes to the alkali metal cations, theoretical calculations were performed using Gaussian 98 [54]. The geometry optimizations and vibrational analyses were performed at the B3LYP/6-31+G* level for all systems that do not contain iodine [55,56]. Note that while benzene and fluorobenzene were previously investigated both experimentally and theoretically, the level of theory employed in those studies differed slightly from that employed here and thus calculations for these systems were also performed even though experiments for these systems were not pursued here. The B3LYP/6-31+G* level of theory was chosen for optimizations, rather than the previously used B3LYP/6-31G* level, because stable B3LYP/6-31G* geometries for all three of the binding conformations of the $K^+(C_6H_5Br)$ complex could not be found. When used to model the data or to calculate thermal energy corrections the B3LYP/6-31+G* vibrational frequencies were scaled by a factor of 0.9804 [57–59]. The vibrational frequencies and rotational constants for the ground state conformations are available as Supplementary Information and are listed in Tables 1S and 2S, respectively. Single point energy calculations were performed at the MP2(full)/6-311+G(2d,2p) level using the B3LYP/6-31+G* optimized geometries. Parameters for iodine are not available in the above basis sets; therefore, calculations for the C_6H_5I systems were performed using a hybrid basis set in which the effective core potentials (ECPs) and valence basis sets of Hay and Wadt were used to describe the halogen [60,61], while the standard basis sets described above were used for all other atoms. These hybrid basis sets will hereafter be referred to as B3LYP/HW/6-31+G* and MP2(full)/HW/6-311+G(2d,2p). To assess the accuracy of these calculations, the C_6H_5Br systems were also computed using the corresponding ECPs for Br. To obtain accurate BDEs, zero point energy (ZPE) corrections were applied and basis set superposition errors (BSSE) were subtracted from the computed BDEs in the full counterpoise correction [62,63]. We carefully considered various possible alkali metal cation binding sites to the halobenzenes, specifically to the π-electron density above the aromatic ring, to the π-electron density above the C–X bond, and to the lone pair of electrons of the halogen substituent, to determine their relative stabilities and the ground state conformations of these complexes.

Polarizability is one of the key factors that influence the strength of cation–π interactions. The experimental polarizabilities of benzene and the halobenzenes have been reported; however, several values have been reported for benzene, chlorobenzene, and bromobenzene that are not in very good agreement. In addition, the polarizabilities of several of the π-ligands used in our binding parameter analysis have not been reported. Thus, to establish a consistent set of polarizabilities for use in this study, the isotropic molecular polarizabilities of benzene, the halobenzenes, and the other π-ligands included in our binding parameter analysis were calculated at the PBE0/6-311+G(2d,2p) level of theory. This level of theory has been shown to accurately reproduce experimental polarizabilities [64].

To more clearly visualize the electronic properties of these ligands and understand the preferences for the various modes of binding, electrostatic potential (ESP) maps of benzene and the halobenzene ligands were calculated at the B3LYP/6-31+G* level of theory. The computed ESP of each of these π-ligands were mapped onto an isosurface of the total SCF electron density (0.005 a.u. for the maps generated in this work). The electrostatic potential maps generated via this procedure were then color-coded according to potential with the regions of most negative electrostatic potential shown in red, and those with the most positive electrostatic potential shown in blue.

2.3. Thermochemical analysis

The threshold regions of the reaction cross sections are modeled using Eq. (1)

$$\sigma(E) = \sigma_0 \sum_i \frac{g_i(E + E_i - E_0)^n}{E} \quad (1)$$

where σ_0 is an energy-independent scaling factor, E is the relative translational energy of the reactants, E_0 is the threshold for reaction of the ground electronic and ro-vibrational state, and n is an adjustable parameter that describes the efficiency of kinetic to internal energy transfer [65]. The summation is over the ro-vibrational states of the reactant ions, i, where E_i is the excitation energy of each ro-vibrational state, and g_i is the population of those states ($\Sigma g_i = 1$). The relative reactivity of all ro-vibrational states, as reflected by σ_0 and n, is assumed to be equivalent.

The Beyer–Swinehart algorithm [66–68] is used to evaluate the density of the ro-vibrational states, and the relative populations, g_i, are calculated for a Maxwell–Boltzmann distribution at 298 K, the internal temperature of the reactants. The vibrational frequencies of the reactant complexes are determined from density functional theory calculations as discussed in Section 2.2. The average vibrational energies at 298 K of the $M^+(C_6H_5X)$ complexes are given in Table 1S in the Supplementary Information. We have estimated the sensitivity of our analysis to the deviations from the true frequencies by increasing and decreasing the computed frequencies (pre-scaled 0.9804) by 10% to encompass the range of average scaling factors needed to bring calculated frequencies

into agreement with experimentally determined frequencies [69,70]. The corresponding change in the average vibrational energy is taken to be an estimate for one standard deviation of the uncertainty in vibrational energy (Table 1S).

We also consider the possibility that the collisionally activated complex ions do not dissociate on the time scale of our experiment ($\sim 10^{-4}$ s) by including statistical theories for unimolecular dissociation, specifically Rice–Ramsperger–Kassel–Marcus (RRKM) theory, into Eq. (1) as described in detail elsewhere [71,72]. The vibrational frequencies appropriate for the energized molecules and the transition states (TSs) leading to dissociation are given in Table 1S. In our analysis, we assume that the TSs are loose and product-like because the interaction between the alkali metal cation and the halobenzene ligand is largely electrostatic (ion-dipole, ion-induced dipole, and ion-quadrupole interactions). In this case, the TS vibrations used are the frequencies corresponding to the products, which are also found in Table 1S. The translational frequencies, those that become rotations of the completely dissociated products, are treated as rotors, a treatment that corresponds to a phase space limit (PSL) and is described in detail elsewhere [71].

The model represented by Eq. (1) is expected to be appropriate for translationally driven reactions [73] and has been found to reproduce CID cross-sections well. The model of Eq. (1) is convoluted with the kinetic-energy distributions of both reactants, and a nonlinear least-squares analysis of the data is performed to give optimized values for the parameters σ_0, E_0, and n. The error associated with the measurement of E_0 is estimated from the range of threshold values determined for the zero-pressure-extrapolated data sets, variations associated with uncertainties in the vibrational frequencies (±10% scaling as discussed above), and the error in the absolute energy scale, 0.05 eV (lab). For analyses that include the RRKM lifetime analysis, the uncertainties in the reported E_0(PSL) values also include the effects of increasing and decreasing the time assumed available for dissociation ($\sim 10^{-4}$ s) by a factor of 2.

Eq. (1) explicitly includes the internal energy of the ion, E_i. All energy available is treated statistically because the energy is redistributed throughout the ro-vibrational modes of the $M^+(C_6H_5X)$ complex upon collision with Xe. Because the CID processes examined here are simple noncovalent bond cleavage reactions, the E_0(PSL) values determined by analysis with Eq. (1) can be equated to 0 K BDEs [74,75].

3. Results

3.1. Cross sections for collision-induced dissociation

Experimental cross sections were obtained for the interaction of Xe with six $M^+(C_6H_5X)$ complexes, where $M^+ = Na^+$ and K^+, and X = Cl, Br, and I. Fig. 2a shows representative data for the $Na^+(C_6H_5Br)$ complex. The other $M^+(C_6H_5X)$ complexes exhibit similar behavior and are shown in Figure 1S in the Supplementary Information. The most favorable process for all complexes over the range of collision energies examined is the loss of the intact halobenzene ligand in the CID reactions (2).

$$M^+(C_6H_5X) + Xe \rightarrow M^+ + C_6H_5X + Xe \quad (2)$$

The magnitudes of the cross sections generally increase from Na^+ to K^+, largely because the thresholds decrease in that same order. Ligand exchange processes to form M^+Xe are also observed as minor reaction pathways, reactions (3).

$$M^+(C_6H_5X) + Xe \rightarrow MXe^+ + C_6H_5X \quad (3)$$

The cross sections for these M^+Xe products are more than two orders of magnitude smaller than those for the primary M^+ product. At elevated energies, loss of NaX thereby producing $C_6H_5^+$ as the ionic product is also observed for the $Na^+(C_6H_5Br)$ and $Na^+(C_6H_5I)$ complexes, reaction (4).

$$M^+(C_6H_5X) + Xe \rightarrow C_6H_5^+ + MX + Xe \quad (4)$$

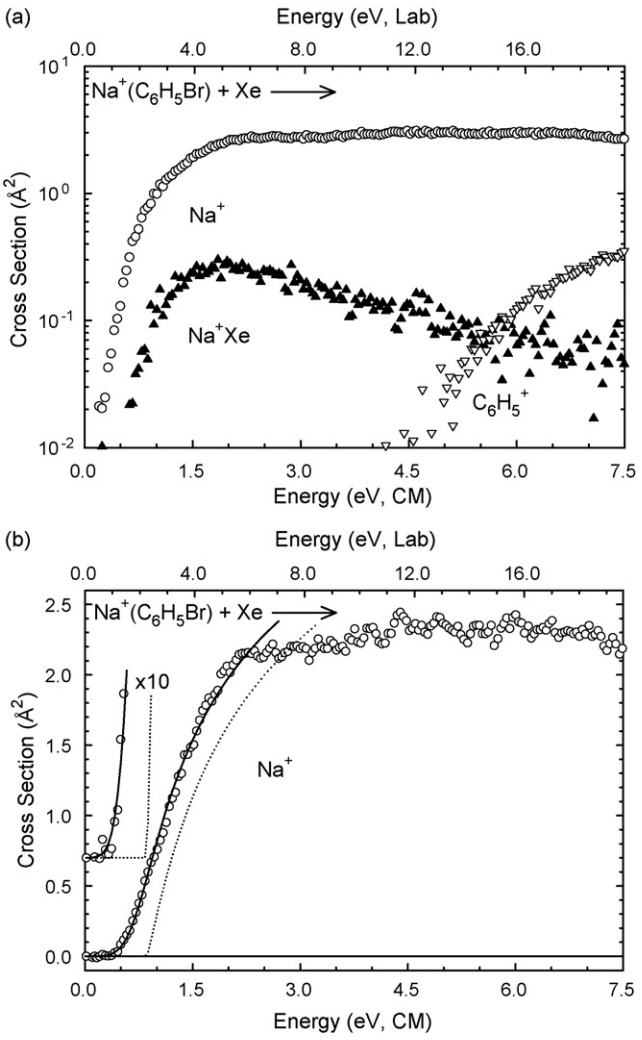

Fig. 2. CID cross sections for $Na^+(C_6H_5Br)$ with Xe as a function of kinetic energy in the center-of-mass frame (lower *x*-axis) and laboratory frame (upper *x*-axis). (a) Data is shown for a Xe pressure of ~0.2 mTorr. The Na^+ and $C_6H_5^+$ products and Na^+Xe ligand exchange cross sections are shown as ○, □, and ▲, respectively. (b) Zero-pressure-extrapolated cross section for the Na^+ product in the threshold region. The solid line shows the best fit to the data using the model of Eq. (1) convoluted over the neutral and ion kinetic and internal energy distributions. The dashed line show the model cross section in the absence of experimental kinetic-energy broadening for reactants with an internal energy corresponding to 0 K.

3.2. Threshold analyses

The model of Eq. (1) was used to analyze the thresholds for reaction (2) in six $M^+(C_6H_5X)$ systems. The results of these analyses are given in Table 1 for all six $M^+(C_6H_5X)$ complexes. Representative results using Eq. (1) for $Na^+(C_6H_5Br)$ are shown in Fig. 2b. The other $M^+(C_6H_5X)$ complexes exhibit similar behavior and are shown in Figure 2S of the Supplementary Information. Experimental cross sections for the M^+ primary dissociation product are accurately reproduced using a loose PSL TS model [71]. This model has been shown to provide the most accurate determination of kinetic shifts for CID reactions of electrostatically bound metal–ligand complexes [71,76]. The data is accurately reproduced over energy ranges exceeding 1 eV and cross-section magnitudes of at least a factor of 100. Threshold values, E_0 and E_0(PSL), obtained from analyses of

Table 1
Fitting parameters of Eq. (1), threshold dissociation energies at 0 K, and entropies of activation at 1000 K[a].

Reactant complex	σ_0[b]	n[b]	E_0 (eV)[c]	E_0(PSL) (eV)	Kinetic shift (eV)	$\Delta S^{\ddagger}$(PSL) (J/(K mol))
$Na^+(C_6H_5Cl)$	1.1 (0.2)	1.0 (0.1)	0.77 (0.04)	0.76 (0.03)	0.01	39 (2)
$K^+(C_6H_5Cl)$	5.5 (0.6)	1.1 (0.3)	0.59 (0.03)	0.58 (0.03)	0.01	32 (2)
$Na^+(C_6H_5Br)$	2.7 (0.1)	1.2 (0.1)	0.85 (0.03)	0.84 (0.03)	0.01	38 (2)
$K^+(C_6H_5Br)$	8.4 (1.2)	1.1 (0.1)	0.69 (0.03)	0.68 (0.03)	0.01	27 (2)
$Na^+(C_6H_5I)$	13.4 (1.2)	1.3 (0.1)	0.91 (0.04)	0.89 (0.04)	0.03	39 (2)
$K^+(C_6H_5I)$	5.1 (0.1)	1.3 (0.1)	0.70 (0.03)	0.70 (0.03)	0.00	33 (2)

[a] Uncertainties are listed in parentheses.
[b] Average values for loose PSL transition state.
[c] No RRKM analysis.

the data without and including explicit consideration of lifetime effects are also included in Table 1. The difference between these threshold values, the kinetic shift, is also given in Table 1. The kinetic shifts observed for these systems are very small, 0.00–0.03 eV, and decrease with increasing size of the alkali metal cation such that they correlate with the strength of binding as expected. For the systems where the π_x conformers are believed to be populated, we also fit the data using the parameters for this conformer. The fitting parameters obtained for these latter analyses were virtually identical to those obtained for fits using the molecular parameters associated with the ground state conformations, and in particular, the E_0(PSL) values differed by <0.01 eV. Thus, only results for the analyses based on the ground state conformations are provided in Table 1 and shown in Figures 2 and 2S.

The entropy of activation, $\Delta S^{\ddagger}$, is a measure of the looseness of the TS, but also depends upon the threshold energy. The $\Delta S^{\ddagger}$(PSL) values at 1000 K are listed in Table 1 and vary between 27 and 39 J/(K mol). These entropies of activation compare favorably to an expanding range of noncovalently bound metal–ligand complexes previously measured in our laboratory [17,19–25,27–31,46] and to those collected by Lifshitz for simple bond cleavage reactions of ions [77].

3.3. Theoretical results

Theoretical structures for the neutral C_6H_5X ligands and $M^+(C_6H_5X)$ complexes, where $M^+ = Na^+$ and K^+, and X = H, F, Cl, Br, and I, were calculated as described in Section 2.2. Key geometrical parameters of the geometry-optimized structures for all of the halobenzene containing species are given in Table 2. The stable structures found for the $Na^+(C_6H_5X)$ complexes are shown in Fig. 3.

3.3.1. Dipole moments of the neutral π-ligands

The measured [45] and B3LYP/6-31+G* calculated dipole moments of benzene and the halobenzenes are shown in Fig. 1. As can be seen in the figure, the dipole moment of C_6H_5F is reproduced quite well, 1.63 D versus 1.60 ± 0.08 D. In contrast, the dipole moments of the heavier halobenzenes all lie outside of the exper-

Table 2
Geometrical parameters of B3LYP/6-31+G* optimized structures of the neutral C_6H_5X ligands and $M^+(C_6H_5X)$ complexes.

Complex		M^+–C (Å)	M^+–R_c[a] (Å)	M^+–⊥ (Å)	Offset (Å)	M^+–X (Å)	C–X (Å)
C_6H_5F							1.361
$Na^+(C_6H_5F)$	π_c	2.812	2.436	2.434	0.000		1.344
$Na^+(C_6H_5F)$	σ					2.119	1.422
$K^+(C_6H_5F)$	π_c	3.293	2.979	2.979	0.000		1.350
$K^+(C_6H_5F)$	σ					2.545	1.408
C_6H_5Cl							1.760
$Na^+(C_6H_5Cl)$	π_c	2.795	2.423	2.423	0.000		1.742
$Na^+(C_6H_5Cl)$	π_x			2.539	1.869		1.780
$Na^+(C_6H_5Cl)$	σ					2.626	1.812
$K^+(C_6H_5Cl)$	π_c	3.289	2.976	2.970	0.189		1.749
$K^+(C_6H_5Cl)$	π_x			3.052	1.971		1.774
$K^+(C_6H_5Cl)$	σ					3.075	1.798
C_6H_5Br							1.904
C_6H_5Br[b]							1.962
$Na^+(C_6H_5Br)$	π_c	2.806	2.432	2.427	0.156		1.900
$Na^+(C_6H_5Br)$	π_c[c]	2.763	2.424	2.423	0.000		1.942
$Na^+(C_6H_5Br)$	π_x			2.577	2.206		1.934
$Na^+(C_6H_5Br)$	π_x[c]			2.567	1.812		1.981
$Na^+(C_6H_5Br)$	σ					2.760	1.957
$Na^+(C_6H_5Br)$	σ[c]					2.797	2.020
$K^+(C_6H_5Br)$	π_c	3.290	2.987	2.964	0.366		1.896
$K^+(C_6H_5Br)$	π_c[c]	3.249	2.933	2.926	0.203		1.958
$K^+(C_6H_5Br)$	π_x			3.014	2.027		1.930
$K^+(C_6H_5Br)$	π_x[c]			3.068	1.515		1.960
$K^+(C_6H_5Br)$	σ					3.206	1.940
$K^+(C_6H_5Br)$	σ[c]					3.100	1.954
C_6H_5I[b]							2.140
$Na^+(C_6H_5I)$	π_c[c]	2.743	2.413	2.412	0.000		2.123
$Na^+(C_6H_5I)$	σ[b]					3.010	2.187
$K^+(C_6H_5I)$	π_c[c]	3.298	2.988	2.965	0.370		2.130
$K^+(C_6H_5I)$	σ[c]					3.539	2.172

[a] The metal-ring centroid distance is defined as the distance from the metal cation to the central point within the aromatic ring of the halobenzene that is in the plane of the carbon atoms.
[b] The offset is defined as the in-plane (parallel) distance the metal atom is displaced from the center of the aromatic ring.
[c] Geometrical parameters of the B3LYP/HW/6-31+G* optimized structures.

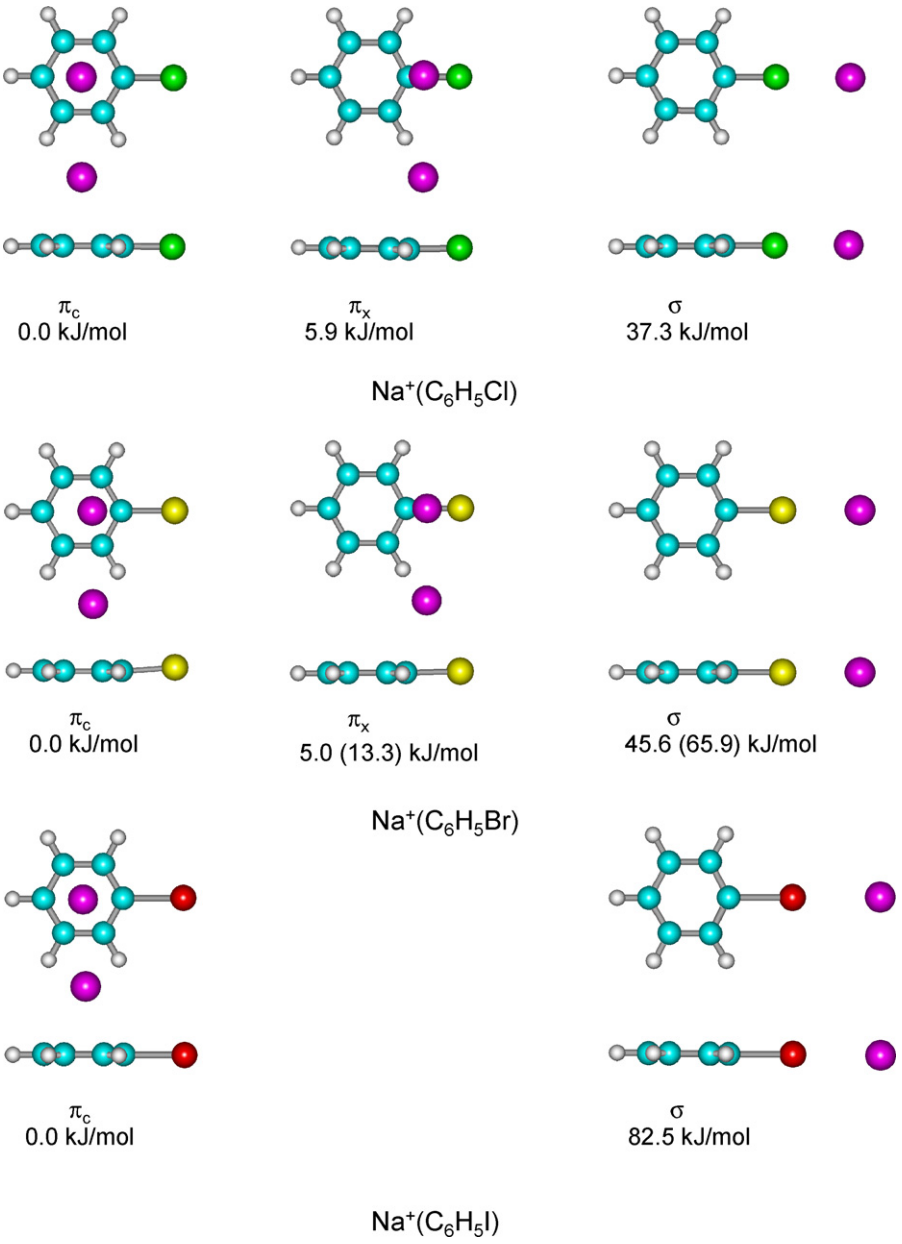

Fig. 3. B3LYP/6-31+G* optimized geometries of the $Na^+(C_6H_5X)$ complexes. Three types of stable geometries are shown, the ground state cation–π conformer (π_c), the cation–π conformer in which Na^+ binds to the halogen substituent (π_x), and the σ-binding conformer in which Na^+ binds to a lone pair of the halogen substituent (σ) Two views of each optimized structure and their MP2(full)/6-311+G(2d,2p)//B3LYP/6-31+G* and MP2(full)/HW/6-311+G(2d,2p)// B3LYP/HW/6-31+G* relative energies including ZPE corrections are shown. For the $Na^+(C_6H_5Br)$ complex, the results using the ECP are given in parentheses.

imental error in the measured values, 1.81 D versus 1.69 ± 0.03 D, 1.86 D versus 1.70 ± 0.03 D, 1.78 D versus 1.70 ± 0.03 D, and 1.50 D versus 1.70 ± 0.08 D for C_6H_5Cl, C_6H_5Br, C_6H_5Br (ECP), and C_6H_5I (ECP), respectively. It is interesting that the use of an ECP provides a better value for C_6H_5Br, but the poorest agreement is found for C_6H_5I, which also uses an ECP. As a result of the poor agreement between the measured and calculated dipole moments, the measured values were used in our binding parameter analyses.

3.3.2. Isotropic molecular polarizabilities of the neutral π-ligands

The measured [45] and PBE0/6-311+G(2d,2p) calculated isotropic molecular polarizabilities are also listed in Fig. 1. The measured values reported in the figure were all derived from one source and happened to be those in the best agreement with the values calculated here. As can be seen in the figure, the polarizability of C_6H_6 is reproduced exactly. Very good agreement between the measured and calculated polarizabilities is also found for C_6H_5F (10.3 Å^3 vs. 10.00 Å^3), C_6H_5Cl (12.3 Å^3 vs. 12.06 Å^3), and C_6H_5Br (13.62 Å^3 vs. 13.39 Å^3). The agreement is not quite as good for C_6H_5I (15.5 Å^3 vs. 14.01 Å^3), but is still within 10%. Because measured polarizabilities are not available for all of the π-ligands included in our binding parameter analyses, the calculated polarizabilities are used in the thermochemical analysis of the experimental data as well as the binding parameter analyses.

3.3.3. Electrostatic potential maps of the neutral π-ligands

The electrostatic potential maps of neutral C_6H_6, C_6H_5F, C_6H_5Cl, C_6H_5Br, and C_6H_5I were calculated as described in Section 2.2 and are shown in Fig. 4. As can be seen in the figure, the regions of greatest electron density (color-coded in red) occur above and below the plane of the aromatic ring as expected based upon the delocalized π-electron density of the aromatic system. In contrast, the

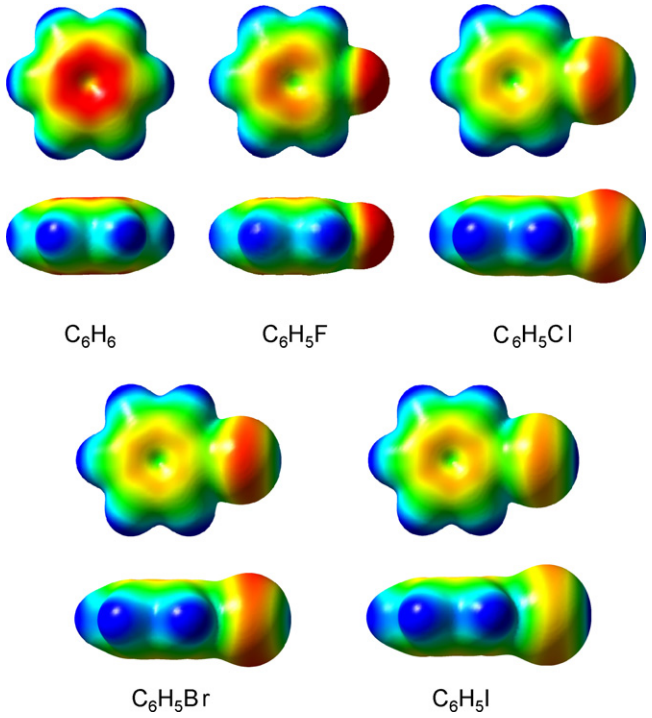

Fig. 4. Electrostatic potential maps of C_6H_6, C_6H_5F, C_6H_5Cl, C_6H_5Br, and C_6H_5I at an isosurface of 0.005 a.u. of the total SCF electron density. Two views for each π-ligand are shown. In the view from above, the molecules are oriented as in Fig. 1.

most electropositive regions (color-coded in blue) occur near the plane of the molecule around the hydrogen atoms. The electron density in the region around the halogen substituent varies with the substituent and is greatest for C_6H_5F due to the highly electronegative F atom, and gradually decreases with the size of the halogen substituent. In addition, the electron density around the halogen substituent is fairly isotropic for C_6H_5F, and becomes less isotropic such that the electron density along the C–X bond becomes increasingly electropositive for the larger halogen substituents. On the basis of the electrostatic potential maps, stable binding modes of the alkali metal cations to the halobenzenes might be expected to the π-electron density above the aromatic ring or C–X bond, and to the lone pairs of the halogen substituent. However, binding in the plane to the halogen substituent becomes increasingly less favorable for the larger halogens.

3.3.4. $M^+(C_6H_5X)$ π_c complexes

In the ground state conformations, π_c, the alkali metal cation binds to the π cloud of the aromatic ring of the C_6H_5X ligand via a cation–π interaction. The C–X bond length was found to decrease upon complexation to the alkali metal cation. The C–X bond lengths change more significantly in the $Na^+(C_6H_5X)$ complexes than the corresponding $K^+(C_6H_5X)$ complexes as a result of the stronger binding interaction. The calculations using full electron correlation for the C_6H_5Br complexes exhibit a smaller decrease in the C–X bond length than the calculations where the ECP is employed. As summarized in Table 2, the M^+–C, M^+–R_c [78], and M^+–⊥ [79] distances are found to increase as the size of the metal cation increases from Na^+ to K^+. These distances are generally found to decrease on going from C_6H_5F to C_6H_5Cl to C_6H_5Br to C_6H_5I, although modest deviations from these trends are observed. In addition, the M^+–C, M^+–R_c, and M^+–⊥ distances of the structures determined using full electron correlation for the C_6H_5Br complexes are larger than the values for the corresponding complexes computed using an ECP for the Br atom. With the exception of $Na^+(C_6H_5Br)$ computed with full electron correlation, the $Na^+(C_6H_5X)$ complexes exhibit no offset of the metal cation from the ring centroid (see Fig. 3). In contrast, the $K^+(C_6H_5X)$ complexes exhibit an offset of the metal cation that follows the order: $C_6H_5I > C_6H_5Br > C_6H_5Cl > C_6H_5F$. As found for the $Na^+(C_6H_5Br)$ complex, the offset of the metal cation is larger for the $K^+(C_6H_5Br)$ complex when full electron correlation is used.

3.3.5. $M^+(C_6H_5X)$ π_x complexes

As can be seen in Fig. 3, the ground state structures of $Na^+(C_6H_5X)$ complexes involve interaction of the Na^+ cation with the π cloud of the aromatic ring such that Na^+ sits at or near the center of the ring, the π_c conformer. However, it is possible that the alkali metal cation might interact with the halogen substituent. Because the halogen substituent is very nearly planar, the lone pair of electrons on the halogen atom are oriented in the direction perpendicular to the plane of the molecule, the direction of the π space. This allows the halogen substituent to delocalize some of its electron density into the π system and increases the resonance stabilization of the halobenzene ligand. Thus, complexes in which the alkali metal cation interacts with the electron density above the C–X bond are also cation–π complexes. Stable cation–π conformers in which the alkali metal cation interacts with the substituent (π_x) were also found for the $M^+(C_6H_5X)$ complexes, where $M^+ = Na^+$ and K^+, and X = Cl and Br. The optimized π_x structures of the $Na^+(C_6H_5X)$ complexes, where X = Cl and Br are also shown in Fig. 3. It is interesting to note that in the π_x complexes, the alkali metal cation is oriented to allow efficient interaction with the dipole moment of the halobenzene ligand. At the MP2(full)/6-311+G(2d,2p) level of theory, the π_x conformers are found to be less stable than the ground state π_c conformers by 5.9 and 4.0 kJ/mol for the $M^+(C_6H_5Cl)$ complexes, 5.7 and 3.8 kJ/mol for the $M^+(C_6H_5Br)$ complexes when full electron correlation is used, and 9.7 and 6.9 kJ/mol when the ECP is used, where $M^+ = Na^+$ and K^+, respectively. The difference in stability of the ground state π_c conformers and the excited π_x conformers suggests that the ion beams generated under our experimental conditions are likely composed of an equilibrium mixture of both conformers (see Table 1S of the Supplementary Information).

3.3.6. $M^+(C_6H_5X)$ σ complexes

It is also possible for the alkali metal cation to interact with a lone pair of electrons on the halogen substituent via a σ-type interaction. Stable σ-binding conformers were also found for all of the $M^+(C_6H_5X)$ complexes. The optimized structures of the σ-binding conformers of the $Na^+(C_6H_5X)$ complexes are also shown in Fig. 3. In the σ-binding complexes, the metal cation lies in the plane of the ring and is oriented along the dipole moment of the halobenzene ligand. At the MP2(full)/6-311+G(2d,2p) level of theory, the σ-binding conformers are found to be 5.8, 37.3, and 45.6 kJ/mol less stable for the $Na^+(C_6H_5X)$ complexes using full electron correlation, where X = F, Cl, and Br, and 65.9 and 82.5 kJ/mol less favorable when an ECP is used to describe the halogen substituent, where X = Br and I, respectively. The σ-binding conformers are found to be 3.6, 28.5, and 34.4 kJ/mol less stable for the $K^+(C_6H_5X)$ complexes using full electron correlation, where X = F, Cl, and Br, and 52.5 and 66.2 kJ/mol less favorable when an ECP is used to describe the halogen substituent, where X = Br and I, respectively. Thus, the relative stabilities of the π_c and π_x conformers are relatively insensitive to the size of the alkali metal cation and halogen substituent. In contrast, the relative stabilities of the π_c and σ-binding conformers are relatively insensitive to the size of the alkali metal cation, but are extremely sensitive to the size of the halogen substituent.

Table 3
Bond dissociation enthalpies of $M^+(C_6H_5X)$, where X = H, F, Cl, Br, and I at 0 K (kJ/mol).

Complex	Experiment (TCID)[a]	Conformer	Theory		
			D_e[b]	D_0[b,c]	$D_{0,BSSE}$[b,d]
$Na^+(C_6H_6)$	92.6 (5.8)[e] 88.3 (4.3)[f]	π_c	104.8	101.0	91.4
$K^+(C_6H_6)$	73.3 (3.8)[e]	π_c	79.9	77.0	71.8
$Na^+(C_6H_5F)$	69.7 (3.3)[g]	π_c	87.1	85.0	75.4
		σ	80.5	79.2	72.9
$K^+(C_6H_5F)$	55.1 (3.0)[g]	π_c	64.7	62.6	57.5
		σ	59.7	59.0	55.5
$Na^+(C_6H_5Cl)$	73.7 (3.4)	π_c	89.3	86.3	76.5
		π_x	82.3	80.4	70.6
		σ	49.3	49.0	43.5
$K^+(C_6H_5Cl)$	56.3 (2.9)	π_c	67.8	65.9	60.3
		π_x	63.0	61.9	56.3
		σ	37.6	37.4	34.2
$Na^+(C_6H_5Br)$	80.6 (3.1)	π_c	90.8	88.7	78.4
		π_c[h]	97.8	94.6	82.6
		π_x	84.3	83.0	73.4
		π_x[h]	87.0	84.9	69.3
		σ	43.1	43.1	37.7
		σ[h]	29.0	28.7	21.9
$K^+(C_6H_5Br)$	65.9 (2.9)	π_c	69.3	67.6	61.8
		π_c[h]	74.9	72.8	65.6
		π_x	65.2	63.8	57.7
		π_x[h]	67.6	65.9	57.5
		σ[h]	33.3	33.2	30.4
		σ	20.4	20.3	15.9
$Na^+(C_6H_5I)$	86.0 (4.2)	π_c[h]	103.7	100.6	87.6
		σ[h]	18.3	18.1	11.0
$K^+(C_6H_5I)$	67.2 (3.0)	π_c[h]	79.2	77.5	69.4
		σ[h]	11.4	11.3	7.6

[a] Threshold collision-induced dissociation, present results except as noted. Uncertainties are listed in parentheses.
[b] Calculated at the MP2(full)/6-311+G(2d,2p)//B3LYP/6-31+G* level of theory.
[c] Including ZPE corrections with B3LYP/6-31+G* or B3LYP/HW/6-31+G* frequencies scaled by 0.9804.
[d] Also includes BSSE corrections.
[e] Amicangelo and Armentrout, Ref. [16].
[f] Armentrout and Rodgers, Ref. [17].
[g] Amunugama and Rodgers, Ref. [21].
[h] Calculated at the MP2(full)/HW/6-311+G(2d,2p)//B3LYP/HW/6-31+G* level of theory.

4. Discussion

4.1. Cation–π complexes: π_c versus π_x binding

As discussed in the Theoretical Results section, both π_c and π_x conformers are found for the $M^+(C_6H_5X)$ complexes, where $M^+ = Na^+$ and K^+, and X = Cl and Br. The relative stabilities of the π_c versus π_x complexes is such that a mixture of the two conformers is likely generated in our source for these $M^+(C_6H_5X)$ complexes because the π_x conformers are only 3.8 to 5.9 kJ/mol less stable than the analogous π_c complexes. However, the calculations performed using the ECP for Br suggest that the relative stabilities differ by a few kJ/mol more and may be as large as 9.7 kJ/mol. The population of the π_x conformers present in our ion beams will tend to lower the measured threshold for CID of these complexes, as can be seen by comparing the measured and calculated BDEs listed in Table 3 (BDEs including ZPE corrections).

The BDEs measured for the $M^+(C_6H_5Cl)$ complexes suggest that the ion beams were composed of a mixture of the π_c and π_x conformers, and that the π_x conformers are present in sufficient abundance to influence the measured threshold. The presence of the π_x conformers does not appear to have significantly influenced the CID threshold for the $M^+(C_6H_5Br)$ complexes (Table 3). The π_x conformers are 9.7 and 6.9 kJ/mol less stable than the π_c complexes for the complexes to Na^+ and K^+ when an ECP is used to describe the Br atom, respectively. The full electron correlation calculations for these complexes suggest that the π_x conformers are relatively more stable such that these conformers are only 4.0 and 3.8 kJ/mol less stable than the ground state π_c conformers, respectively. It is also interesting to note that no π_x conformers for the $M^+(C_6H_5Br)$ complexes were found when optimizations were performed at the B3LYP/6-31G* level of theory. Stable π_x conformers were not found for the C_6H_5F and C_6H_5I complexes for either level of theory, B3LYP/6-31G* or B3LYP/6-31+G*. Computations for the C_6H_5I complex always converged to the more stable π_c conformer. This result is not surprising based upon the ESP maps, which show that the electron density in the region above the C–X bond is much reduced as compared to that of C_6H_5Cl and C_6H_5Br. In contrast, the C_6H_5F complexes always converged to σ conformers. This result is again consistent with the ESP map of C_6H_5F, which shows greater electron density near the fluoro-substituent than above the C–F bond.

4.2. σ-Binding versus cation–π complexes

Stable conformers in which the alkali metal cation binds to the lone pair of electrons of the halogen substituent, σ conformers, were found for all the $M^+(C_6H_5X)$ complexes. The σ conformers become increasingly less stable as the size of the halogen increases, and are 5.8, 37.3, and 45.6 kJ/mol less stable for the $Na^+(C_6H_5X)$ complexes calculated using full electron correlation, and 65.9 and 82.5 kJ/mol less favorable when an ECP is used to describe the halogen substituent. Similarly, the σ conformers are 3.6, 28.5, and 34.4 kJ/mol less stable for the $K^+(C_6H_5X)$ complexes using full electron correlation, and 52.5 and 66.2 kJ/mol less stable when an ECP is used to describe the halogen substituent. The measured threshold for CID of the $M^+(C_6H_5F)$ systems [21] are lowered due to the presence of the σ conformers in the ion beams generated (Table 3). The σ conformers for the other systems are not expected to have such an effect on the measured threshold for CID, because they are more than 28 kJ/mol less stable than the corresponding π_c complexes, and thus should not be present in an appreciable population for these systems.

4.3. Comparison of theory and experiment

The experimentally determined and theoretically calculated M^+-C_6H_5X BDEs at 0 K, where X = H, F, Cl, Br, and I and $M^+ = Na^+$ and K^+ are summarized in Table 3. The agreement between the experimental BDEs and theoretical values determined at the MP2(full)/6-311+G(2d,2p)//B3LYP/6-31+G* and MP2(full)/HW/6-311+G(2d,2p)//B3LYP/HW/6-31+G* levels is illustrated in Fig. 5. The theoretical values plotted in Fig. 5 represent the thermally weighted averages of the BDEs calculated for a 298 K Maxwell–Boltzmann distribution. Thus, in addition to the ground state π_c conformations, the σ conformer for the $M^+(C_6H_5F)$ complexes and the π_x conformers for $M^+(C_6H_5Cl)$ and $M^+(C_6H_5Br)$ complexes are included because the ion beams generated under our experimental conditions should be comprised of a statistical mixture of these ground state and low energy conformations. Consistent with the halouracil systems previously studied [80], the agreement between the experimental BDEs and the theoretical values using the ECP for the C_6H_5Br complexes is better than that found for the values computed using full electron correlation. The mean absolute deviation (MAD) [81] between the measured BDEs and the values calculated using full electron correlation, (i.e., the $M^+(C_6H_5Cl)$ and $M^+(C_6H_5Br)$ complexes) for the ground state π_c conformers is 3.3 ± 0.9 kJ/mol. The MAD is almost unaffected when the thermally weighted values are used, and becomes 3.3 ± 1.1 kJ/mol. The MAD is somewhat better for the values calculated using the ECP, (i.e., the $M^+(C_6H_5Br)$ and $M^+(C_6H_5I)$ complexes) for the ground state π_c conformers is 1.5 ± 0.9 kJ/mol, and improves slightly when the thermally weighted values are used and becomes 1.3 ± 0.9 kJ/mol.

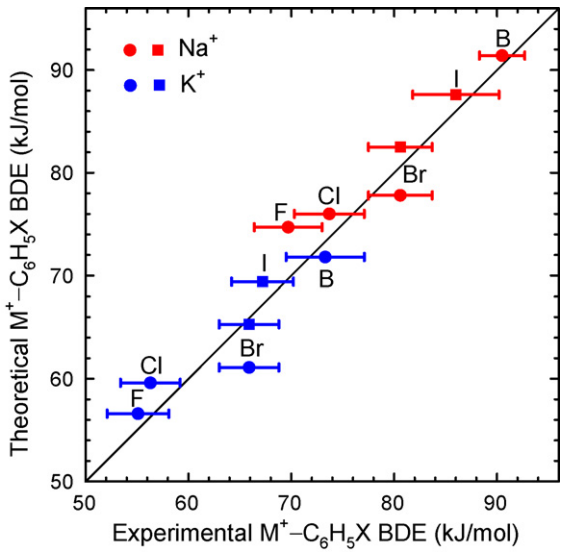

Fig. 5. Weighted theoretical versus experimental BDEs at 0 K (in kJ/mol) of the $M^+(C_6H_5X)$ complexes. The diagonal line indicates the values for which the calculated and measured BDEs are equal. Values obtained from MP2(full)/6-311+G(2d,2p) and MP2(full)/HW/6-311+G(2d,2p) level of theory are shown as ● and ■, respectively.

When the best computed values are used for all six complexes (i.e., the thermally weighted values and those computed using the ECP as appropriate) is quite good, 2.0 ± 0.9 kJ/mol. In all cases, these MADs are similar or better than the average experimental uncertainty (AEU) in these values of 3.3 ± 0.5 kJ/mol. Thus, the M^+-C_6H_5X BDEs measured here provide reliable anchors for the alkali metal cation affinity scales.

4.4. Conversion from 0 to 298 K

The 0 K BDEs determined here are converted to 298 K bond enthalpies and free energies. The enthalpy and entropy conversions are calculated using standard formulas (assuming harmonic oscillator and rigid rotor models), and the vibrational and rotational constants determined for the B3LYP/6-31+G* optimized geometries given in Tables 1S and 2S in the Supplementary Information. Table 4 lists 0 and 298 K enthalpies, free energies, and enthalpic and entropic corrections for all systems experimentally determined and taken from Table 3. The uncertainties in the enthalpic and entropic corrections are determined by 10% variation in the molecular constants. Because the metal cation–ligand frequencies are very low and may not be adequately described by theory, the listed uncertainties also include contributions from scaling these low-frequency modes up and down by a factor of two. The latter provides a conservative estimate of the computational error in the uncertainties listed.

4.5. Influence of the size of the alkali metal cation

The experimental BDEs of the $M^+(C_6H_5X)$ complexes are summarized in Table 3. The BDEs for these complexes are found to decrease as the size of the alkali metal cation increases from Na^+ to K^+. Similar behavior was also found for the analogous cation–π complexes to C_6H_6 [14,76], toluene ($C_6H_5CH_3$) [20], C_6H_5F [21], phenol (C_6H_5OH) [22], anisole ($C_6H_5OCH_3$) [23], naphthalene ($C_{10}H_8$) [24], indole (C_8H_7N) [28], pyrrole (C_4H_4NH) [15,18,29], 1-methylpyrrole ($C_4H_4NCH_3$) [19], aniline ($C_6H_5NH_2$) [25], *N*-methylaniline ($C_6H_5NHCH_3$) [31], and *N*,*N*-dimethylaniline ($C_6H_5N(CH_3)_2$) [31] previously investigated. This is the expected trend for binding based primarily on electrostatic interactions (ion-dipole, ion-quadrupole, and ion-induced dipole) [9,82,83], because the increasing size of the alkali metal cation leads to larger metal cation–ligand bond distances (see Table 2).

4.6. The influence of the halogen substituent

The effect of the halogen substituent on the cation–π interaction can be examined by comparing the results obtained here for C_6H_5Cl, C_6H_5Br, and C_6H_5I, to those obtained in earlier studies for C_6H_6 [15] and C_6H_5F [21]. As a result of the high degree of symmetry, benzene exhibits no dipole moment. The halogens are electron-withdrawing substituents that reduce the symmetry of the molecule and result in a fairly large dipole moment for all of the halobenzenes, Fig. 1. As a result of the reduction in the π-electron density of the aromatic ring, cation–π complexes of the halobenzenes are expected to exhibit weaker binding than benzene. Indeed, both the measured and calculated BDEs of the $M^+(C_6H_5F)_x$ complexes previously determined are weaker than the corresponding $M^+(C_6H_6)_x$ complexes, where $M^+ = Li^+$, Na^+, K^+, Rb^+ and Cs^+ and $x = 1–2$ [21]. As can be seen in Fig. 6, the $M^+(C_6H_5X)$ complexes examined here also exhibit weaker binding than the corresponding $M^+(C_6H_6)$ complexes, where $M^+ = Na^+$ and K^+ and X = Cl, Br, and I. The anticipated trend in the binding among the halobenzenes is not quite as obvious. The electron-withdrawing character of the halogen substituents should correlate with their electronegativities, which follow the order F (3.98) > Cl (3.16) > Br (2.96) > I (2.66) [45]. Indeed, both the measured and calculated M^+–C_6H_5X BDEs exhibit an inverse correlation with the electronegativities of the halogen substituent as can be seen in Fig. 7. Earlier work by Dougherty and co-workers [9,10,84,85] and our group [18–31] has shown that cation–π interactions are dominated by the ion-quadrupole interaction, which depends upon the π-electron density. Therefore, the M^+-C_6H_5X BDEs might be expected to follow the order F < Cl < Br < I. However, the measured dipole moments of the halobenzenes exhibit less variation than might be expected based on the electronegativities of the halogen substituents and follow the order, C_6H_5F (1.60 ± 0.08 D) < C_6H_5Cl (1.69 ± 0.03 D) < C_6H_5Br (1.70 ± 0.03 D) ≈ C_6H_5I (1.70 ± 0.09 D) [45]. Thus, the π-electron density of all of the halobenzenes should

Table 4
Enthalpies and free energies of binding of $M^+(C_6H_5X)$, where X = Cl, Br, and I, at 0 and 298 K (kJ/mol)[a].

Reactant complex	ΔH_0[b]	$\Delta H_{298} - \Delta H_0$[c]	ΔH_{298}	$T\Delta S_{298}$[c]	ΔG_{298}
$Na^+(C_6H_5Cl)$	73.7 (3.4)	1.0 (0.7)	74.7 (3.5)	29.6 (2.1)	45.1 (4.1)
$K^+(C_6H_5Cl)$	56.3 (2.9)	0.3 (1.6)	56.6 (3.3)	27.9 (4.9)	28.7 (5.9)
$Na^+(C_6H_5Br)$[d]	80.6 (3.1)	0.9 (1.2)	81.5 (3.3)	29.5 (3.7)	52.0 (5.0)
$K^+(C_6H_5Br)$[d]	65.9 (2.9)	0.3 (0.7)	66.2 (3.0)	27.1 (4.2)	39.1 (5.2)
$Na^+(C_6H_5I)$[d]	86.0 (4.2)	1.0 (1.3)	87.0 (4.4)	29.8 (3.7)	57.2 (5.7)
$K^+(C_6H_5I)$[d]	67.2 (3.0)	0.3 (1.0)	67.5 (3.2)	28.1 (4.1)	39.4 (5.2)

[a] Uncertainties are listed in parentheses.
[b] Present experimental results taken from Table 3.
[c] Density functional values from calculations at B3LYP/6-31+G* level of theory with frequencies scaled by 0.9804.
[d] Values from calculations at the B3LYP/HW/6-31+G* level of theory with frequencies scaled by 0.9804.

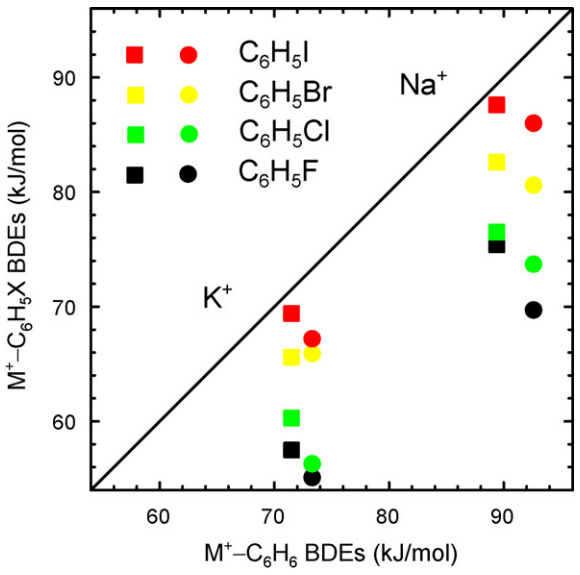

Fig. 6. Bond dissociation energies (in kJ/mol) at 0 K of the $M^+(C_6H_5X)$ versus $M^+(C_6H_6)$ complexes, where X = F, Cl, Br, and I, and $M^+ = Na^+$ and K^+. Measured values are shown as circles, while calculated values are shown as squares. Values for C_6H_6 are taken from Ref. [16]. Values for C_6H_5F are taken from Ref. [21].

be depleted relative to benzene, but fluorobenzene would be expected to the least π deficient, while the other halobenzenes would be expected to exhibit very similar π deficiencies. In this case, the M^+-C_6H_5X BDEs might be expected to follow the order I ≈ Br ≈ Cl < F. However, to completely rationalize the trends in the binding among the halobenzenes, ion-induced dipole interactions, which depend upon the polarizability of the π-ligand, must also be considered. The measured polarizabilities of the halobenzenes increase with increasing size of the halogen substituent, C_6H_5F (10.3 Å^3) < C_6H_5Cl (12.3 Å^3) < C_6H_5Br (13.62 Å^3) < C_6H_5I (15.5 Å^3) [45]. Thus, the strength of the ion-induced dipole interaction should increase in this same order. As can be seen in Figs. 6 and 7, the M^+-C_6H_5X BDEs follow the order F < Cl < Br < I, in agreement with expectations based upon the electronegativities of the halogens and polarizabilities of the halobenzenes. However, the dipole moments of the halobenzenes should be more indicative of the strength of the ion-quadrupole interactions within these complexes, and thus the observed trend in the M^+-C_6H_5X BDEs arises as a result of the cumulative ion-quadrupole and ion-induced

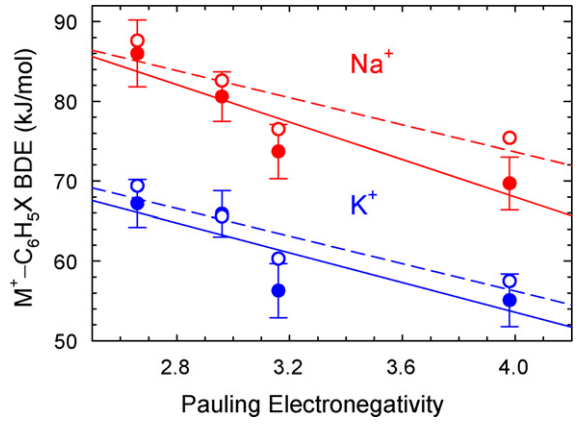

Fig. 7. Bond dissociation energies (in kJ/mol) at 0 K of the $M^+(C_6H_5X)$ complexes versus the Pauling electronegativity of the halogen substituent. Experimental values are shown as closed symbols and solid lines, while theoretical values are shown as open symbols and dashed lines. The lines are linear regression fits to the data.

dipole contributions to the binding and lead to an increase in the strength of the binding as the size of the halogen substituent increases.

4.7. Nature of the cation–π interaction

Noncovalent interactions such as cation–π interactions are the result of a combination of ion-quadrupole, ion-dipole, and ion-induced dipole interactions. In order to elucidate the detailed contributions that each of the above interactions contribute to the strength of the binding in cation–π complexes, we have carried out studies in which the alkali metal cation and π-ligands were systematically varied. By performing a detailed numerical analysis based upon the binding parameter model of Eq. (5), estimates for the relative and absolute contributions of these three interactions to the binding were determined.

$$\mathrm{BDE}\,(M^+\text{-}\pi\text{-ligand}) = e(M^+)\,\{a[Q(B) + b \times D_{//}(\pi\text{-ligand})] + c \times D_{\perp}(\pi\text{-ligand}) + d \times \alpha(\pi\text{-ligand})\} \quad (5)$$

In this equation, the fitting parameters a, b, c, and d are all independent of the metal cation and the total BDE is scaled for each metal cation using the parameter $e(M^+)$. This yields a family of equivalent fits to the data for which we arbitrarily set $e(Li^+)$ to unity. The first term, $a[Q(B) + b \times D_{//}(\pi\text{-ligand})]$ represents the contribution of the ion-quadrupole interaction to the binding, where $Q(B)$ is the quadrupole moment of benzene (−8.69 D Å) [86], the only ligand amongst this set that has been experimentally determined, and $D_{//}$ is the in-plane (parallel) component of the dipole moment of the π-ligand. The electron donating (or withdrawing) effects of the substituent lead to an increase or decrease in the π-electron density of the aromatic ring and thereby enhance (or reduce) the quadrupole moment of the π-ligand. Similarly, the contributions of ion-dipole and ion-induced dipole interactions are estimated by the $c \times D_{\perp}(\pi\text{-ligand})$ and $d \times \alpha$ (π-ligand) terms, respectively, where $D_{\perp}$ is the perpendicular component of the dipole moment and α is the polarizability of each π-ligand. Measured values for the dipole moments of each ligand were used, while the parallel and perpendicular components of the dipole moments of aniline, *N*-methylaniline, and *N*,*N*-dimethylaniline were calculated using the measured dipole moments and the dipole orientations obtained from theoretical calculations. Similarly, calculated π-ligand polarizabilities were used as measured values were not available for the entire π-ligand set. The measured dipole moments, and $D_{//}$, $D_{\perp}$, and α values for all π-ligands investigated to date are summarized in Table 3S of the Supporting Information. The absolute and relative contributions of these three cation–π interactions for each $M^+(\pi\text{-ligand})$ complex were determined using a weighted analysis of the experimental and theoretical bond energies. For the analysis based on the theoretical results, the uncertainties assumed were 14, 8, 8, 12, and 12 kJ/mol for the complexes to Li^+, Na^+, K^+, Rb^+, and Cs^+, respectively. The values for Li^+ and Na^+ are representative of the uncertainties previously found in comparisons between experiment and theory [17,87]. Values for K^+ were estimated to match those of Na^+, whereas those for Rb^+ and Cs^+ were set higher because of the use of the effective core potentials.

Our published work to date [19–25,28,29,31] has examined five alkali metal cations including: Li^+, Na^+, K^+, Rb^+ and Cs^+ and 11 π-ligands including: toluene, fluorobenzene, aniline, phenol, anisole, naphthalene, indole, pyrrole, 1-methylpyrrole, *N*-methylaniline, and *N*,*N*-dimethylaniline. Results from Amicangelo and Armentrout [16] for benzene are also included in our analyses. In the present study, the set of π-ligands is extended to include chlorobenzene, bromobenzene, and iodobenzene to further elucidate the inductive effects of halogenation on the strength of cation–π interactions. The analysis carried out here includes a total of 64 distinct $M^+(\pi\text{-ligand})$

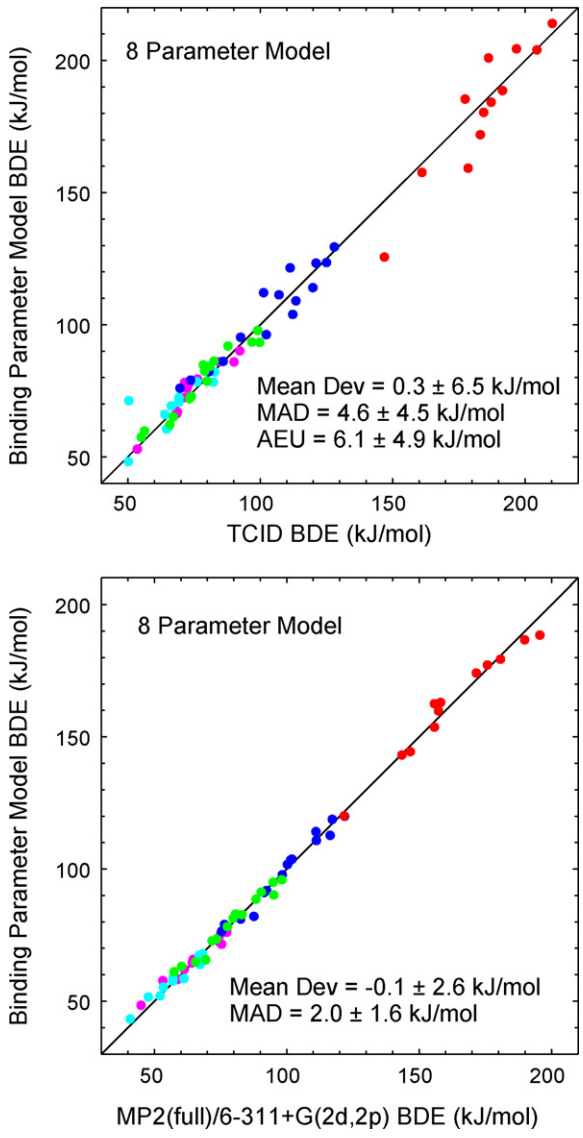

Fig. 8. TCID measured (a) and MP2(full)/6-311+G(2d,2p) (b) BDEs versus BDEs predicted using the binding parameter model of Eq. (5) for 64 M^+(π-ligand) complexes, where M^+ = Li^+ (●), Na^+ (●) K^+ (●), Rb^+ (●), and Cs^+ (●) and π-ligand = benzene [17], toluene [20], fluorobenzene [21], chlorobenzene, bromobenzene, iodobenzene, phenol [22], anisole [23], naphthalene [24], indole [28], pyrrole [19,29], 1-methylpyrrole [19], aniline [25], *N*-methylaniline [31], and *N*,*N*-dimethylaniline [31]. The diagonal line indicates the values for which the measure (or calculated) and predicted values are equal.

complexes. The fitting parameters thus obtained are summarized in Table 4S of the Supplementary Information. Overall, this approach reproduces the experimental data with a MAD of 4.6 ± 4.5 kJ/mol and a mean deviation of 0.3 ± 6.5 kJ/mol. The AEU in these values, 6.1 ± 4.9 kJ/mol, is somewhat larger than the MAD for the fit to the data. Predictions for the MP2(full)/6-311+G(2d,2p) calculated BDEs lead to an even smaller MAD of 2.0 ± 1.6 kJ/mol and a mean deviation of −0.1 ± 2.6 kJ/mol. The overall reproduction of the data is illustrated in Fig. 8. As can be seen in the figure, the calculated values are reproduced with high fidelity using this model. The fit to the experimental results shows evidence of a few outliers, a likely results of the independent nature of each measurement and variable magnitudes of the experimental error for each measurement.

The absolute and relative ion-quadrupole, ion-induced dipole, and ion-dipole contributions to the cation–π interactions obtained from the analyses of the measured and calculated M^+–π-ligand BDEs are listed in Tables 5S and 6S of the Supplementary Information, respectively. As a result of the nature of the binding parameter model of Eq. (5) used to analyze the data, the absolute ion-quadrupole, ion-induced dipole, and ion-dipole contributions to the cation–π interaction are constrained to increase linearly with increasing estimated quadrupole moment, polarizability, and the magnitude of the perpendicular component of the dipole moment of the π-ligand, respectively. The model also ensures that the contributions of each of these interactions to the M^+–π-ligand BDE are zero when the quadrupole moment, polarizability, or dipole moment are zero. As can be seen in Tables 5S and 6S, each of these interactions decrease with the size of the alkali metal cation for all ligands. This behavior is expected because the alkali metal cation–π-ligand bond distance increases with the size of the alkali metal cation, and these interactions scale as R^{-3}, R^{-4}, and R^{-2}, respectively. The *e* parameter of Eq. (5) indicates that the average ratio of the BDEs for the complexes to Li^+, Na^+, K^+, Rb^+, and Cs^+ are 1.0:0.60:0.46:0.42:0.38 from the analysis of the experimental data, and 1:0:0.64:0.51:0.40:0.36 from the analyses of the calculated BDEs. These are remarkably similar to the ratios obtained for a wide variety of ligands previously investigated [82,83].

The results of this binding parameter model suggest that the binding is indeed dominated by the ion-quadrupole interaction. The relative contributions derived from fits to the experimental data vary between 63 and 86%, while theory suggests that this interaction is even more important, and varies between 71 and 88% across these 15 π-ligands. The ion-quadrupole contributions for chlorobenzene (69 and 75%), bromobenzene (66 and 73%), and iodobenzene (63 and 72%) are amongst the smallest, a result of the electron-withdrawing (inductive) effects of the halogen substituent (experiment and theory, respectively). Ion-induced dipole interactions are also found to be important contributors to the binding and account for 15 to 37% and 12 to 28% of the measured and calculated BDEs, respectively. The ion-induced dipole contributions for chlorobenzene (31 and 25%), bromobenzene (34 and 27%) and iodobenzene (37 and 28%) are amongst the largest, as a result of the enhancement in the polarizability induced by the halogen substituent. The trends amongst the other π-ligands are very similar to that found in our previous analysis of the smaller π-ligand set [31]. Ion-dipole effects on the binding depend strongly on the orientation of the molecular dipole moment. The parallel (in-plane) component of the dipole moment serves to increase or decrease the π-electron density of the aromatic ring and thus results in an increase or decrease in the strength of the ion-quadrupole interaction. For the π-ligands with a nonzero perpendicular component of the dipole moment, (i.e., aniline, *N*-methylaniline, and *N*,*N*-dimethylaniline) ion-dipole interactions also contribute to the binding. The relative contributions derived from fits to the experimental data vary between 2 and 6%, while theory suggests that this interaction is somewhat more important and varies between 3 and 12%, across these three π-ligands. It should be noted that the ion-perpendicular dipole interactions appear to reduce the relative contributions of the ion-quadrupole interactions but not the ion-induced dipole interactions.

The binding parameter model analyses also allow estimates of the quadrupole moments of these π-ligands to be extracted. Estimated quadrupole moments based upon the analyses of the experimental and calculated values are listed in Table 5. The estimated quadrupole moments for these π-ligands exhibit good agreement with quantitative and semi-quantitative predictions of the influence of the substituent on the π-electron density of the aromatic ring, supporting the validity of the model. The values estimated here are all within the estimated uncertainties of the quadrupole moments previously determined for the smaller π-ligand set. The inclusion of chlorobenzene, bromobenzene, and iodobenzene (as well as 1-methylpyrrole) in the binding parameter analysis, led to a modest increase in the estimated quadrupole

Table 5
Estimated quadrupole moments of the neutral π-ligands (in D Å)[a].

Ligand	Estimated quadrupole moment	
	TCID[b]	MP2(full)[c]
C_6H_5I	−6.30 (0.26)	−6.88 (0.24)
C_6H_5Br	−6.30 (0.26)	−6.88 (0.24)
C_6H_5Cl	−6.31 (0.26)	−6.89 (0.24)
C_6H_5F	−6.44 (0.24)	−6.98 (0.23)
C_6H_5OH	−8.61 (0.01)	−8.63 (0.01)
$C_6H_5CH_3$	−9.21 (0.06)	−9.09 (0.05)
$C_6H_5OCH_3$	−9.61 (0.10)	−9.38 (0.09)
$C_6H_5NH_2$	−9.68 (0.11)	−9.44 (0.10)
$C_6H_5NHCH_3$	−10.53 (0.20)	−10.09 (0.19)
C_8H_7N	−10.79 (0.23)	−10.28 (0.21)
$C_6H_5N(CH_3)_2$	−11.03 (0.26)	−10.46 (0.24)
C_4H_4NH	−11.18 (0.27)	−10.58 (0.26)
$C_4H_4NCH_3$	−11.77 (0.33)	−11.03 (0.31)

[a] Uncertainties are listed in parentheses.
[b] Values estimated using TCID measured BDEs.
[c] Values estimated using BDEs computed at the MP2(full)/6-311+G(2d,2p) or MP2(full)/HW/6-311+G(2d,2p) levels of theory for all M^+(π-ligand) complexes except the $Li^+(C_6H_5NH_2)$, $Li^+(C_6H_5NHCH_3)$, and $Li^+(C_6H_5N(CH_3)_2)$ complexes, where G3 values are used.

moment of fluorobenzene and very slight decreases for the nitrogen containing π-ligands that are π-enhanced relative to benzene. The estimated quadrupole moments of C_6H_5Cl, C_6H_5Br, and C_6H_5I are essentially equal, a result of the nearly equal dipole moments of these π-ligands.

5. Conclusions

The kinetic-energy dependences of the CID of $M^+(C_6H_5X)$ complexes, where $M^+ = Na^+$, and K^+, and X = Cl, Br, and I, with Xe are examined in a guided ion beam tandem mass spectrometer. The dominant dissociation pathway observed for all complexes is loss of the intact halobenzene ligand. The thresholds for these primary dissociation reactions are interpreted to extract 0 and 298 K BDEs. The molecular parameters needed for analysis of experimental data, as well as structures and theoretical estimates of the BDEs for the $M^+(C_6H_5X)$ complexes are obtained from theoretical calculations performed at the MP2(full)/6-311+G(2d,2p)//B3LYP/6-31+G* and MP2(full)/HW-6-311+G(2d,2p)//B3LYP/HW/6-31+G* levels of theory. The agreement between theory and experiment is very good for all complexes. The absolute M^+-C_6H_5X BDEs are observed to decrease as the size of the alkali metal cation increases from Na^+ to K^+, and increase as the size of the halogen increases from F to I. These trends arise from the electrostatic nature of the bonding and the inductive and polarization effects of the halogen substituent. The absolute and relative contributions of the ion-quadrupole and ion-induced dipole interactions to the binding of these $M^+(C_6H_5X)$ complexes are determined via numerical analysis, and vary from 63 to 69% and 31 to 37% based on the measured BDEs, and 72 to 75% and 25 to 28% based on the calculated BDEs, respectively. Estimates for the quadrupole moments of C_6H_5Cl, C_6H_5Br, and C_6H_5I are obtained from the same numerical analysis and exhibit good agreement with qualitative and semi-quantitative predictions of the inductive effect of the halogen substituents. Comparison of the present results to the analogous benzene and fluorobenzene systems reveals that the inductive effects of the halogen substituent result in cation–π interactions that are intermediary between benzene and fluorobenzene for both alkali metal cations.

Acknowledgments

This work is supported by the National Science Foundation, Grant CHE-0518262 and the American Chemical Society Petroleum Research Fund, Grant 40334-AC6. The authors also thank Wayne State University C&IT for computer time. EU would also like to thank the Wayne State University Honors program for financial support.

Appendix A. Supplementary data

Supplementary data associated with this article can be found, in the online version, at doi:10.1016/j.ijms.2009.01.006.

References

[1] S.-H. Liaw, I. Kuo, D. Eisenberg, Protein Sci. 4 (1995) 2358.
[2] A.R.C. Raine, C.-C. Yang, L.C. Packman, S.A. White, F.S. Mathews, N.S. Scrutton, Protein Sci. 4 (1995) 2625.
[3] J. Wouters, Protein Sci. 7 (1998) 2472.
[4] G. Labesse, D. Ferrari, Z.-w. Chen, G.-L. Rossi, V. Kuusk, W.S. McIntire, F.S. Mathews, J. Biol. Chem. 273 (1998) 25703.
[5] R. MacKinnon, G. Yellen, Science 250 (1990) 276.
[6] L. Heginbotham, R. MacKinnon, Neuron 8 (1992) 483.
[7] L. Heginbotham, Z. Lu, T. Abramson, R. MacKinnon, Biophys. J. 66 (1994) 1061.
[8] G.W. Gokel, L.J. Barbour, S.L. De Wall, E.S. Meadows, Chem. Rev. 222 (2001) 127.
[9] J.C. Ma, D.A. Dougherty, Chem. Rev. 97 (1997) 1303.
[10] D.A. Dougherty, Science 271 (1996) 163.
[11] R.L. Nakamura, J.A. Anderson, R.F. Gaber, J. Biol. Chem. 272 (1997) 1011.
[12] G.W. Gokel, L.J. Barbour, R. Ferdani, J. Hu, Acc. Chem. Res. 35 (2002) 878.
[13] V. Ryzhov, R.C. Dunbar, J. Am. Chem. Soc. 121 (1999) 2259.
[14] V. Ryzhov, R.C. Dunbar, B. Cerda, C. Wesdemiotis, J. Am. Soc. Mass Spectrom. 11 (2000) 1037.
[15] A. Gapeev, C.-N. Yang, S.J. Klippenstein, R.C. Dunbar, J. Phys. Chem. A 104 (2000) 3246.
[16] J.C. Amicangelo, P.B. Armentrout, J. Phys. Chem. A 104 (2000) 11420.
[17] P.B. Armentrout, M.T. Rodgers, J. Phys. Chem. A 104 (2000) 2238.
[18] A. Gapeev, R.C. Dunbar, J. Am. Chem. Soc. 123 (2001) 8360.
[19] H. Huang, M.T. Rodgers, J. Phys. Chem. A 106 (2002) 4277.
[20] R. Amunugama, M.T. Rodgers, J. Phys. Chem. A 106 (2002) 5529.
[21] R. Amunugama, M.T. Rodgers, J. Phys. Chem. A 106 (2002) 9092.
[22] R. Amunugama, M.T. Rodgers, J. Phys. Chem. A 106 (2002) 9718.
[23] R. Amunugama, M.T. Rodgers, Int. J. Mass Spectrom. 222 (2003) 431.
[24] R. Amunugama, M.T. Rodgers, Int. J. Mass Spectrom. 227 (2003) 1.
[25] R. Amunugama, M.T. Rodgers, Int. J. Mass Spectrom. 227 (2003) 339.
[26] R.L. Grimm, J.B. Mangrum, R.C. Dunbar, J. Phys. Chem. A 108 (2004) 10897.
[27] C. Ruan, M.T. Rodgers, J. Am. Chem. Soc. 126 (2004) 14600.
[28] C. Ruan, Z. Yang, N. Hallowita, M.T. Rodgers, J. Phys. Chem. A 109 (2005) 11539.
[29] C. Ruan, Z. Yang, M.T. Rodgers, Int. J. Mass Spectrom. 267 (2007) 233.
[30] C. Ruan, Z. Yang, M.T. Rodgers, Phys. Chem. Chem. Phys. 9 (2007) 5902.
[31] N. Hallowita, D.R. Carl, P.B. Armentrout, M.T. Rodgers, J. Phys. Chem. A 112 (2008) 7996.
[32] S. Mecozzi, P.A. West Jr., D.A. Dougherty, Proc. Natl. Acad. Sci. U.S.A. 93 (1996) 10566.
[33] R.C. Dunbar, J. Phys. Chem. A 102 (1998) 8946.
[34] R.C. Dunbar, J. Phys. Chem. A 104 (2000) 8067.
[35] D. Feller, D.A. Dixon, J.B. Nicholas, J. Phys. Chem. A 104 (2000) 11414.
[36] S. Ikuta, Mol. J. Struct. (Theochem) 530 (2000) 201.
[37] S. Tsuzuki, M. Yoshida, T. Uchimaru, M. Mikami, J. Phys. Chem. A 105 (2001) 769.
[38] J.M. Vollmer, A.K. Kandalam, L.A. Curtiss, J. Phys. Chem. A 106 (2002) 9533.
[39] R.C. Dunbar, J. Phys. Chem. A 106 (2002) 7328.
[40] S.E. Rodriguez-Cruz, E.R. Williams, J. Am. Soc. Mass Spectrom. 12 (2001) 250.
[41] O.M. Cabarcos, C.J. Weinheimer, J.M. Lisy, J. Chem. Phys. 110 (1999) 8429.
[42] S. Mecozzi, A.P. West Jr., D.A. Dougherty, J. Am. Chem. Soc. 118 (1996) 2307.
[43] C.A. Hunter, C.M. Low, C. Rotger, J.G. Vinter, C. Zonta, Proc. Natl. Acad. Sci. U.S.A. 99 (2002) 4873.
[44] P. Auffinger, F.A. Hays, E. Westhof, P.S. Ho, Proc. Natl. Acad. Sci. U.S.A. 101 (2004) 16789.
[45] D.R. Lide (Ed.), CRC Handbook of Chemistry and Physics, 88th ed., CRC Press, Taylor & Francis, 2007/2008 http://www/hbcpnetbase.com/.
[46] M.T. Rodgers, J. Phys. Chem. A 105 (2001) 8145.
[47] N.F. Dalleska, K. Honma, L.S. Sunderlin, P.B. Armentrout, J. Am. Chem. Soc. 116 (1994) 3519.
[48] N. Aristov, P.B. Armentrout, J. Phys. Chem. 90 (1986) 5135.
[49] D.A. Hales, P.B. Armentrout, J. Cluster Sci. 1 (1990) 127.
[50] E. Teloy, D. Gerlich, Chem. Phys. 4 (1974) 417.
[51] D. Gerlich, Diplomarbeit, University of Freiburg, Federal Republic of Germany, 1971.
[52] D. Gerlich, in: C.-Y. Ng, M. Baer (Eds.), Advances in Chemical Physics Series, vol. 82, Wiley, New York, 1992, p. 1.
[53] K.M. Ervin, P.B. Armentrout, J. Chem. Phys. 83 (1985) 166.
[54] M.J. Frisch, G.W. Trucks, H.B. Schlegel, G.E. Scuseria, M.A. Robb, J.R. Cheeseman, V.G. Zakrzewski, J.A. Montgomery Jr., R.E. Stratmann, J.C. Burant, S. Dapprich, J.M. Millam, A.D. Daniels, K.N. Kudin, M.C. Strain, O. Farkas, J. Tomasi, V. Barone, M. Cossi, R. Cammi, B. Mennucci, C. Pomelli, C. Adamo, S. Clifford, J. Ochterski, G.A. Petersson, P.Y. Ayala, Q. Cui, K. Morokuma, D.K. Malick, A.D. Rabuck, K. Raghavachari, J.B. Foresman, J. Cioslowski, J.V. Ortiz, B.B. Stefanov, G. Liu, A. Liashenko, P. Piskora, I. Komaromi, R. Gomperts, R.L. Matin, D.J. Fox, T. Keith,

M.A. Al-Laham, C.Y. Peng, A. Nanayakkara, C. Gonzalez, M. Challacombe, P.M.W. Gill, B. Johnson, W. Chen, M.W. Wong, J.L. Andres, C. Gonzales, M. Head-Gordon, E.S. Replogle, J.A. Pople, Gaussian 98, Revision A. 11, Gaussian, Inc., Pittsburgh, PA, 1998.
[55] C. Lee, W. Yang, R.G. Parr, Phys. Rev. B 37 (1988) 785.
[56] A.D. Becke, J. Chem. Phys. 98 (1993) 5648.
[57] J.B. Foresman, Æ Frisch, Exploring Chemistry with Electronic Structure Methods, 2nd ed., Gaussian, Pittsburgh, 1996, p. 64.
[58] A.P. Scott, L. Radom, J. Phys. Chem. 100 (1996) 16502.
[59] M.W. Wong, Chem. Phys. Lett. 256 (1996) 391.
[60] The Hay-Wadt valence basis set and effective core potentials were obtained from the Extensible Computational Chemistry Environment Basis Set Database (available on the Internet at http://www.emsl.pnl.gov/forms/basisform.html), as developed and distributed by the Molecular Science Computing Facility, Environmental and Molecular Sciences Laboratory, which is part of the Pacific Northwest National Laboratory, P.O. Box 999, Richland, WA 99352, and funded by the U.S. Department of Energy. For the original valence basis set and ECP reference, see reference [61].
[61] P.J. Hay, W.R. Wadt, J. Chem. Phys. 82 (1985) 284.
[62] S.F. Boys, R. Bernardi, Mol. Phys. 19 (1979) 553.
[63] F.B. van Duijneveldt, J.G.C.N. van Duijneveldt-van de Rijt, J.H. van Lenthe, Chem. Rev. 94 (1994) 1873.
[64] S.M. Smith, A.N. Markevitch, D.A. Romanov, X. Li, R.J. Levis, H.B. Schlegel, J. Phys. Chem. A 108 (2000) 11063.
[65] F. Muntean, P.B. Armentrout, J. Chem. Phys. 115 (2001) 1213.
[66] T.S. Beyer, D.F. Swinehart, Commun. ACM 16 (1973) 379.
[67] S.E. Stein, B.S. Rabinovitch, J. Chem. Phys. 58 (1973) 2438.
[68] S.E. Stein, B.S. Rabinovitch, Chem. Phys. Lett. 49 (1977) 183.
[69] J.A. Pople, H.B. Schlegel, K. Raghavachari, D.J. DeFrees, Int. J. Quantum Chem. Symp. 15 (1981) 269.
[70] D.J. DeFrees, A.D. McLean, J. Chem. Phys. 82 (1985) 333.
[71] M.T. Rodgers, K.M. Ervin, P.B. Armentrout, J. Chem. Phys. 106 (1997) 4499.
[72] F.A. Khan, D.E. Clemmer, R.H. Schultz, P.B. Armentrout, J. Phys. Chem. 97 (1993) 7978.
[73] W.J. Chesnavich, M.T. Bowers, J. Phys. Chem. 83 (1979) 900.
[74] See, for example Figure 1 in N.F. Dalleska, K. Honma, P.B. Armentrout, J. Am. Chem. Soc. 115 (1993) 12125.
[75] P.B. Armentrout, J. Simons, J. Am. Chem. Soc. 114 (1992) 8627.
[76] M.T. Rodgers, P.B. Armentrout, J. Phys. Chem. A 101 (1997) 2614.
[77] C. Lifshitz, Adv. Mass Spectrom. 11 (1989) 113.
[78] The metal-ring centroid distance (M^+–R_c) is defined as the distance from the metal cation to the central point within the aromatic ring that lies in the place of the carbon atoms.
[79] The metal cation-perpendicular distance (M^+–⊥) is defined from the metal cation to the plane of the aromatic ring.
[80] Z. Yang, M.T. Rodgers, J. Am. Chem. Soc. 126 (2004) 16217.
[81] MADs are reported as the mean absolute deviation and one standard deviation in the MAD.
[82] M.T. Rodgers, P.B. Armentrout, Mass Spectrom. Rev. 19 (2000) 215.
[83] M.T. Rodgers, P.B. Armentrout, Acc. Chem. Res. 37 (2004) 989.
[84] S. Mecozzi, P.A. West Jr., D.A. Dougherty, J. Am. Chem. Soc. 118 (1996) 2307.
[85] J.P. Gallivan, D.A. Dougherty, Proc. Natl. Acad. Sci. U.S.A. 96 (1999) 9459.
[86] J.H. Williams, Acc. Chem. Res. 26 (1993) 593, http://www.chemsoc.org/viselements/pages/data/intro_groupi_data.html.
[87] M.T. Rodgers, P.B. Armentrout, Int. J. Mass Spectrom. 267 (2007) 167.